



ISTITUTO NAZIONALE DI RICERCA METROLOGICA Repository Istituzionale

3D nanoSQUID based on tunnel nano-junctions with an energy sensitivity of 1.3 h at 4.2 K

Original

3D nanoSQUID based on tunnel nano-junctions with an energy sensitivity of 1.3 h at 4.2 K / Schmelz, M.; Vettoliere, A.; Zakosarenko, V.; De Leo, N.; Fretto, M.; Stolz, R.; Granata, C.. - In: APPLIED PHYSICS LETTERS. - ISSN 0003-6951. - 111:3(2017), p. 032604. [10.1063/1.4986655]

Availability:

This version is available at: 11696/57072 since: 2018-02-02T10:19:58Z

Publisher:

American Institute of Physics

Published

DOI:10.1063/1.4986655

Terms of use:

This article is made available under terms and conditions as specified in the corresponding bibliographic description in the repository

Publisher copyright

(Article begins on next page)

3D nanoSQUID based on tunnel nano-junctions with an energy sensitivity of 1.3 h at 4.2 K

M. Schmelz, A. Vettoliere, V. Zakosarenko, N. De Leo, M. Fretto, R. Stolz, and C. Granata

Citation: [Appl. Phys. Lett.](#) **111**, 032604 (2017);

View online: <https://doi.org/10.1063/1.4986655>

View Table of Contents: <http://aip.scitation.org/toc/apl/111/3>

Published by the [American Institute of Physics](#)

Articles you may be interested in

[Frequency-multiplexed bias and readout of a 16-pixel superconducting nanowire single-photon detector array](#)
Applied Physics Letters **111**, 032603 (2017); 10.1063/1.4993779

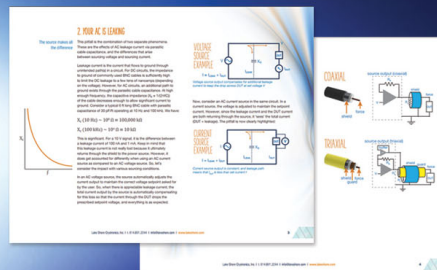
[Overlap junctions for high coherence superconducting qubits](#)
Applied Physics Letters **111**, 032602 (2017); 10.1063/1.4993937

[Multi-frequency spin manipulation using rapidly tunable superconducting coplanar waveguide microresonators](#)
Applied Physics Letters **111**, 032601 (2017); 10.1063/1.4993930

[Microstrip superconducting quantum interference device amplifier: Operation in higher-order modes](#)
Applied Physics Letters **111**, 042604 (2017); 10.1063/1.4985384

[Super-resolution thermographic imaging using blind structured illumination](#)
Applied Physics Letters **111**, 031908 (2017); 10.1063/1.4995410

[Low spin wave damping in the insulating chiral magnet \$\text{Cu}_2\text{OSeO}_3\$](#)
Applied Physics Letters **111**, 032408 (2017); 10.1063/1.4995240



5 Electronic Measurement Pitfalls to Avoid

Get the whitepaper

3D nanoSQUID based on tunnel nano-junctions with an energy sensitivity of $1.3 \hbar$ at 4.2 K

M. Schmelz,¹ A. Vettoliere,² V. Zakosarenko,³ N. De Leo,⁴ M. Fretto,⁴ R. Stolz,¹ and C. Granata^{2,a)}

¹Leibniz Institute of Photonic Technology, PO Box 100239, D-07702 Jena, Germany

²Istituto di Scienze Applicate e Sistemi Intelligenti del CNR, I-80078 Pozzuoli, Italy

³Supracon AG, An der Lehmgrube 11, D-07751 Jena, Germany

⁴Istituto Nazionale di Ricerca Metrologica, I-10135 Torino, Italy

(Received 6 June 2017; accepted 3 July 2017; published online 21 July 2017)

We report the performance of a reliable three-dimensional nanometer-sized Superconducting QUantum Interference Device (SQUID). The use of superconductor-isolator-superconductor Nb/Al-AIO_x/Nb Josephson tunnel junctions together with small SQUID loop dimensions permits a high modulation depth of the SQUID's critical current and thus leads to very low intrinsic flux noise of the device. In particular, we present electrical characterization including detailed noise investigations. At 4.2 K, two-stage noise measurements with a SQUID as a low noise preamplifier result in a white flux noise of $51 \text{ n}\Phi_0/\text{Hz}^{1/2}$, which is equivalent to an energy resolution of $1.3 \hbar$, with \hbar being Planck's constant. Simulation of spin sensitivities results in about $1 \mu\text{B}/\text{Hz}^{1/2}$ for an electron spin positioned directly above the SQUID ring. *Published by AIP Publishing.*
<http://dx.doi.org/10.1063/1.4986655>

In recent years, nanomagnetism is one of the most promising and interesting chapters in matter physics.¹ In this regard, one of the most stimulating challenges for Superconducting Quantum Interference devices (SQUIDs) is the detection of a single electron spin offering the possibility to explore new stimulating nanoscience topics such as the study of single electrons, molecular magnets, and reversal magnetization of a single or few nanoparticles.²⁻⁴ The principle of such a SQUID measurement can be summarized as follows: magnetization variation of a magnetic object produces a magnetic flux change, which is proportional to the magnetization by a coupling factor depending on the geometry of the SQUID pick-up loop and the sample.^{2,4} Note that the SQUID capability to detect magnetic moment or spin is inversely proportional to the size of the pickup loop. In fact, if we suppose to put a magnetic object inside the loop, only the magnetic flux lines, which do not return within the loop, give a net contribution to the magnetic flux. Accordingly, by decreasing the loop size, the net magnetic flux increases, thus favoring small SQUID loop dimensions for this task.

Although efforts for the realization of *nano*-SQUIDs began more than ten years ago, their roots date back to the early eighties of the last century. In a pioneering work, Voss *et al.*⁵ developed niobium dc SQUIDs based on microbridges to reach an energy resolution close to the limit of the uncertainty principle. Some years later, Ketchen *et al.*⁶ proposed a miniature SQUID susceptometer to measure the magnetic properties of micron size samples at low temperature. They introduced the spin sensitivity $S_n^{1/2} = S_\Phi^{1/2}/\Phi_\mu$ as a figure of merit in order to quantitatively evaluate the noise in terms of spin or elementary magnetic moment (Bohr magneton) and demonstrate that it is inversely proportional to the

diameter of the SQUID loop. Here, Φ_μ is the magnetic coupling factor and S_Φ is the flux noise of the SQUID. In 2003, Lam and Tilbrook resumed the original Ketchen's proposal and developed the first nanoSQUID for the detection of small spin populations, having a hole with a side length of 200 nm.⁷ Thereafter, several nanoSQUIDs have been developed, in which main types are based on single layer nano-bridges⁷⁻¹¹ or on sandwich nano-junctions.¹²⁻¹⁷

In this letter, we report detailed electrical transport and magnetic flux noise measurements of a three dimensional (3D) nanoSQUID based on tunnel nano-junctions. This approach combines deep submicron loop dimensions with highly reliable superconductor-isolator-superconductor Josephson tunnel junctions.

The sensor is composed of a capture loop of $0.2 \mu\text{m}^2$ pick up area interrupted by two nanometric Josephson tunnel junctions with an area of $0.09 \mu\text{m}^2$. The detailed fabrication procedure of this nanodevice is reported elsewhere,^{15,18} so only an outline of the main fabrication steps and the differences with respect to the previous fabrication procedure are reported here. The 3D nanoSQUID is realized by merging the robust Nb/Al technology with the Gallium based focused ion beam (FIB) patterning technique being able to realize a three-dimensional device by opportunely sculpting materials through a multistep etching.

Josephson tunnel junctions are based on *in-situ* sputter deposited Nb/Al-AIO_x/Nb thin-films. The two Nb layers, representing the superconducting electrodes, are deposited with a thickness of 300 nm, while the tunneling barrier is an Al-AIO_x bilayer wherein the Aluminum is a 6 nm normal metal layer at a working temperature of 4.2 K. It is sputtered at high deposition rates (1.3 nm/s), and its corresponding thin oxide is obtained through a controlled oxidation into the sputtering chamber with a relatively low oxygen exposure ($E = \text{pressure} \times \text{time}$) of 3700 Pa s. In this specific case, the thickness of the

^{a)}Author to whom correspondence should be addressed: c.granata@cib.na.cnr.it

normal metal represents a good compromise such that the aluminum is not proximized by the adjacent Niobium and, at the same time, the superconducting tunneling effect is guaranteed. The deposited Nb/Al-AlO_x/Nb multilayer is then patterned by a lift-off technique and consequently 3D milled by a focalised gallium ion beam in a FEI Company Quanta 3D dual beam system. The Ga⁺ beam is orthogonally driven on the sputtered Nb/Al structure by a CAD design previously generated. The main fabrication steps and a scanning electron micrograph of the 3D nanoSQUIDs are shown in Fig. 1. In a first step, the FIB patterning results in a rectangular hole in a niobium trilayer strip defining both the SQUID loop and width of the junctions. Next, the sample is tilted by 90° with respect to the ion beam, and other two holes are etched. The trilayer strip width, as well as the hole dimension (300 nm), defines the junction dimensions.

Device characterization has been carried out at 4.2 K with the SQUID being immersed in liquid helium inside a cylindrical lead and outer μ -metal shield. The used dipstick moreover comprises a superconducting solenoid from NbTi wire inside the shields used to provide the magnetic background field to set up the working point of the SQUID and to measure its effective flux capturing area. For the measurement, the chip has been assembled in such orientation that the magnetic field of the solenoid points perpendicular to the chip surface.

Figure 2 shows the measured current-voltage characteristics for different values of magnetic flux threading the SQUID loop (top) and a set of flux-voltage characteristics of the device, where the bias current was increased in steps of 10 μ A ranging from 80 to 250 μ A. From the period of the characteristics together with the prior determined transfer function of the solenoid of about 33 mT/A, we estimate the effective SQUID area A_{eff} of about $3.0 \mu\text{m}^2$. This value is larger than expected from the sensor's geometrical dimensions, as can be seen in Fig. 1, which is most likely caused by the associated flux focusing effects and the non-flat geometry of the SQUID loop. In fact, even if the modulation magnetic field is applied perpendicular to the chip plane, a contribution to the effective area of the component perpendicular to the

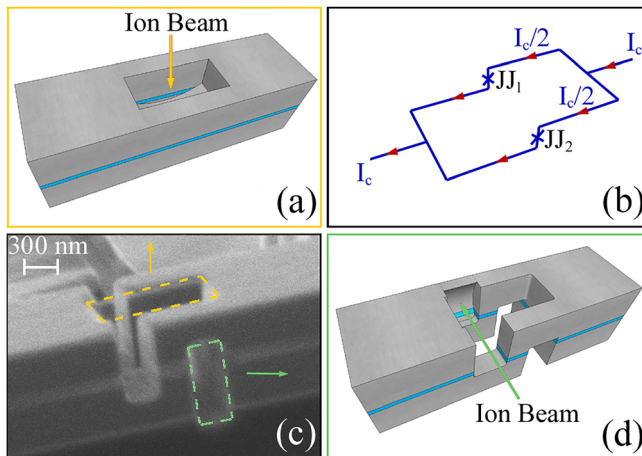


FIG. 1. (a) and (d) Sketches of fabrication steps by the Focused Ion Beam sculpting process. (b) Circuitual scheme of the nanoSQUID in which the current path is highlighted. (c) Scanning electron micrograph of the 3D nanoSQUID.

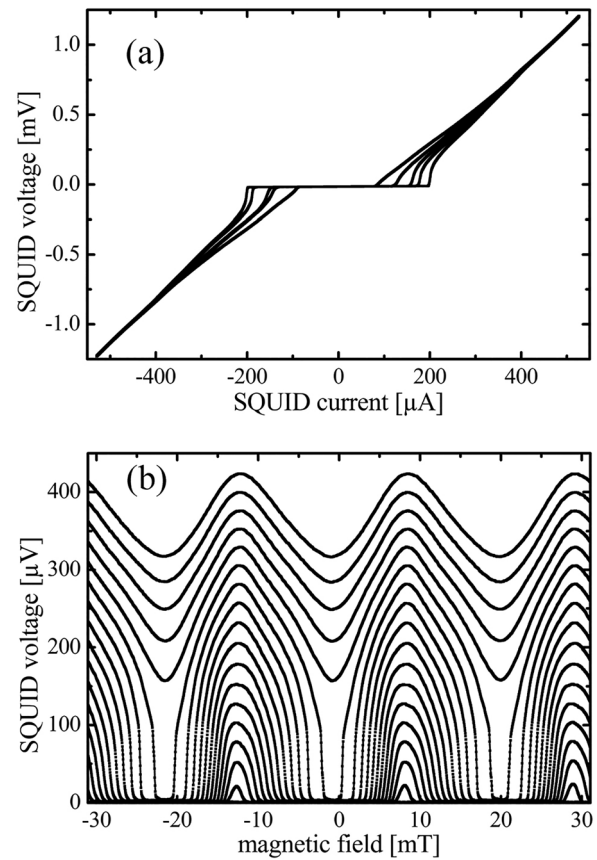


FIG. 2. Set of current-voltage characteristics measured at 4.2 K for different magnetic flux threading the SQUID loop, ranging from 0 to $0.5 \Phi_0$ in steps of $0.1 \Phi_0$ (top) and set of flux-voltage characteristics with stepwise increasing bias current, ranging from 80 to 250 μ A in steps of 10 μ A (bottom).

chip surface [Fig. 1(b)] due to the magnetic field misalignment should be not negligible. However, the value is consistent to prior measurements using a different setup.¹⁹

The SQUID exhibits a maximum critical current of $2I_C = 202 \mu\text{A}$ and a normal state resistance of $R_N/2 = 2.45 \Omega$, with I_C being the critical current of one Josephson junction. The $I_C R_N$ product accordingly results in about 500 μV . The critical current and voltage swing were as large as 118 μA and 310 μV , respectively, which is equivalent to a normalized critical current swing of $\Delta I_C/I_C \approx 0.59$. Accordingly, the modulation parameter $\beta_L = 2L_{SQ}I_0/\Phi_0$ and the SQUID inductance L_{SQ} can be estimated to be about $\beta_L \approx 0.63$ and $L_{SQ} \approx 6.5 \text{ pH}$.²⁰

The investigated device does not exhibit hysteresis for temperatures higher than 4 K, wherefrom therein a junction capacitance of about $C_{JJ} = 60 \text{ fF}$ has been deduced.

It is worth noting that the device characteristics did not change significantly compared to first preliminary investigations,¹⁹ which were done more than one year ago—a major advantage of the fabricated nanoSQUIDs compared to typical counterparts based on constriction type junctions, which typically suffer from poor long term stability mainly against thermal cycling.

From the flux-voltage characteristics, as shown in Fig. 2, a transfer function V_Φ of up to $5 \text{ mV}/\Phi_0$ was deduced. Taking into account the input voltage noise of a low-noise SQUID electronics²¹ of about $S_V^{1/2} = 0.33 \text{ nV/Hz}^{1/2}$, the

noise contribution of the room-temperature electronics in a single stage configuration thus amounts to minimum $S_V^{1/2}/V_\Phi = 66 \text{ n}\Phi_0/\text{Hz}^{1/2}$ what is remarkably higher than the theoretically estimated intrinsic flux noise of only a few tens of $\text{n}\Phi_0/\text{Hz}^{1/2}$ based on the switching current distribution of the SQUID from the zero voltage state results.¹⁹

In order to investigate the intrinsic noise properties of this nanoSQUID, a two-stage noise measurement setup with a SQUID as a low-noise preamplifier as described in Ref. 22 has been used. Here, the SQUID under investigation is voltage-biased with a resistor $R = 1.5 \text{ }\Omega$ in parallel. The critical current change of the nanoSQUIDs is sensed with the amplifier SQUID. Feedback from a low-noise directly coupled SQUID electronics from Supracon AG²¹ has been applied to the amplifier SQUID, and hence, the amplifier SQUID was operated as an ammeter. The amplifier SQUID is a low inductance parallel gradiometer with two washers. It exhibits a low input coil inductance and an input current noise of about $5 \text{ pA}/\text{Hz}^{1/2}$. The flux in the nanoSQUID has been adjusted via the superconducting solenoid so that the measured overall transfer function due to a signal to the nanoSQUIDs was maximum. The persistent current in the solenoid maintained the working point of the SQUID, while the solenoid was disconnected from its room-temperature control electronics during noise measurements. The output of the SQUID electronics has been recorded with a HP 3565 spectrum analyzer with a maximum bandwidth of 100 kHz.

The gray line in Fig. 3 shows the flux noise spectral density of the SQUID measured at 4.2 K. For this figure, the contribution of the amplifier SQUID together with the room-temperature electronics of about $20 \text{ n}\Phi_0/\text{Hz}^{1/2}$ for frequencies larger than $f \approx 10 \text{ Hz}$ has been subtracted. The flux noise spectrum can be fitted by $S_\Phi^{1/2} = 51 \text{ n}\Phi_0/\text{Hz}^{1/2} \cdot [1 + (f_{c1}/f) + (A/(1 + \{f/f_{c2}\}^2))]^{1/2}$, with $f_{c1} = 3.5 \text{ kHz}$, $A = 1200$, and $f_{c2} = 10 \text{ Hz}$, shown as a dashed black line in Fig. 3. The white flux noise accordingly amounts to $51 \text{ n}\Phi_0/\text{Hz}^{1/2}$ corresponding to an energy resolution of the nanoSQUIDs of $\varepsilon = S_\Phi/(2L_{SQ}) \approx 1.3 \text{ h}$ with h being Planck's constant.

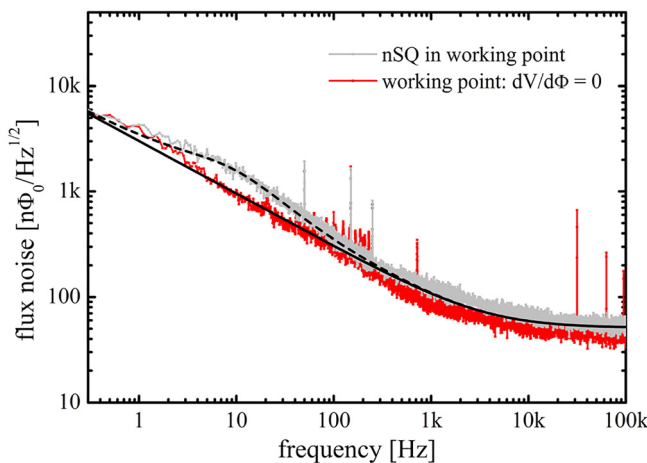


FIG. 3. Flux noise spectral density of the investigated SQUID measured at 4.2 K using a two-stage setup with a SQUID as a low noise preamplifier (gray line), and the corresponding fit is shown as a dashed black line. In magnetic insensitive working points, a behavior according to the red line has been observed, indicating critical current fluctuations as the main reason for the degraded low-frequency noise performance.

Besides this extremely low white noise, an increase at low frequencies is observed. More precisely, there seems to be at least two independent low frequency noise sources with different frequency dependences. Measurements in magnetic insensitive working points with $dV/d\Phi = 0$, shown as a red line in Fig. 3, reveal that the main part of this noise is due to critical current fluctuation in the Josephson junctions, which are already visible as jumps in the time-trace of the recorded output of the SQUID electronics. In such a working point, the fit reduces to $S_\Phi^{1/2} = 51 \text{ n}\Phi_0/\text{Hz}^{1/2} \cdot [1 + (f_{c1}/f)]^{1/2}$, with $f_{c1} = 3.5 \text{ kHz}$, shown as a solid black line in Fig. 3.

Accordingly, the kink at about 10 Hz is due to a magnetic signal threading the SQUID loop, probably due to some normal conducting material or a single fluctuator close to the SQUID.

Nevertheless, at 10 Hz and 1 Hz, the magnitude of flux noise amounts to $1.5 \text{ }\mu\Phi_0/\text{Hz}^{1/2}$ and $4.1 \text{ }\mu\Phi_0/\text{Hz}^{1/2}$, respectively. Despite the very large critical current density of the used Josephson junctions, the nanoSQUIDs do not show significant degradation compared to typical dc SQUIDs based on Josephson junctions with much lower critical current density.

In order to compare our measurements with theoretical predictions, we use the widely known relation of white flux noise

$$S_\Phi^{1/2} = 4L_{SQ}^{3/4}C_{JJ}^{1/4}(2k_B T)^{1/2}$$

for optimized SQUIDs with the McCumber parameter $\beta_C = 2\pi I_C R^2 C_{JJ}/\Phi_0$ and β_L about unity.²³ Accordingly, for the presented device, the estimated white flux noise level amounts to about $42 \text{ n}\Phi_0/\text{Hz}^{1/2}$ at 4.2 K, which is in excellent agreement with our measurements. These results are, moreover, consistent with predictions based on the switching current distribution of the SQUID from the zero voltage state as reported in Ref. 19.

The measured white noise level of the nanoSQUIDs is one of the lowest achieved with SQUIDs so far and in this way continues the quest for quantum limited SQUIDs started already several decades ago.^{5,11,24–26} Notably, the measured white noise is just a factor four larger than the quantum noise limit given as $[h/(2\pi) \cdot L_{SQ}]^{1/2} \approx 13 \text{ n}\Phi_0/\text{Hz}^{1/2}$ for this device.

Since one of the most important applications of nanoSQUIDs is magnetism at the nanoscale, such as the study of the magnetic nano-object, an important figure of merit is the spin or magnetic moment sensitivity as given above. An estimation of Φ_μ can be obtained by using the filamentary model.^{27,28} In this case, the magnetic flux coupled to the SQUID is given by the integral of the vector potential along the SQUID loop border. In Fig. 4, we report the spin sensitivity distribution obtained by varying the position of a particle with a magnetic moment of Bohr magneton μ_B within the nanoSQUID loop. It is computed for three different distances $d = 10, 20$, and 30 nm from the SQUID top loop and considering the experimental determined white magnetic noise of $51 \text{ n}\Phi_0/\text{Hz}^{1/2}$. It is worth noting that the bottom SQUID loop does give a negligible contribution because the distance between the two loops is about 300 nm (top layer thickness). For this distance, the coupled magnetic flux is much smaller than the one coupled to the top SQUID loop²⁷

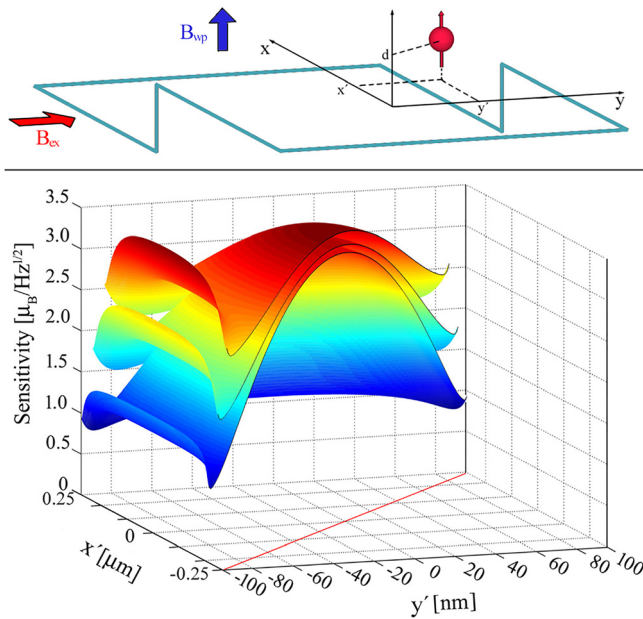


FIG. 4. Simulated spin sensitivity as a function of the position within the half nanoSQUID loop for three different distances (10 nm, 20 nm, and 30 nm) of particle with the magnetic moment of Bohr magneton from the loop plane. In order to display the larger variations, the cut was made along the loop diagonal. In the sketch, the position, the distance with respect to the folded coil, as well as the excitation field (B_{exc}) and the field to adjust the SQUID working point (B_{wp}) are shown.

In order to perform the nanomagnetism measurement, it is possible to apply an excitation field B_{exc} parallel to both the chip plane and the component perpendicular to the chip surface without coupling magnetic flux in the nanoSQUID flux capture area, while an adjusting working point field B_{wp} can be applied perpendicular to the chip surface (see the sketch in Fig. 4). Of course, a little misalignment is unavoidable, so in a practical case, a parasitic signal will be present and a suitable compensation technique should be employed.²⁹

As expected, the best spin sensitivity is obtained close to the edges and at the corners of the SQUID loop. For a distance of 10 nm, which is a reasonable value from the experimental point of view, a spin sensitivity of about $1 \mu_B/\text{Hz}^{1/2}$ is obtained. By increasing the distance, the sensitivity decreases and the dependence from the position within the loop tends to disappear.

In conclusion, we presented a detailed characterization of a robust and reliable 3D nanoSQUID, showing an energy sensitivity approaching the quantum limit at liquid helium temperature. The ultra-low noise magnetic flux together with submicron loop dimensions results in a spin sensitivity of about $1 \mu_B$ per unit bandwidth, indicating the suitability for nanomagnetism applications requiring both high sensitivity and submicron spatial resolution. These results definitely

demonstrate that there are no more barriers for the most sensitive applications such as the detection of individual atomic magnetic moments.

- ¹S. D. Bader, *Rev. Mod. Phys.* **78**, 1 (2006).
- ²C. Granata and A. Vettoliere, *Phys. Rep.* **614**, 1 (2016).
- ³L. Hao and C. Granata, *Supercond. Sci. Technol.* **30**, 0050301 (2017).
- ⁴W. Wernsdorfer, *Supercond. Sci. Technol.* **22**, 064013 (2009).
- ⁵R. F. Voss, R. B. Laibowitz, and A. N. Broers, *Appl. Phys. Lett.* **37**, 656 (1980).
- ⁶M. B. Ketchen, D. D. Awschalom, W. J. Gallagher, A. W. Kleinsasser, R. L. Sandstrom, J. R. Bozen, and B. Bumble, *IEEE Trans. Magn.* **25**, 1212 (1989).
- ⁷S. K. H. Lam and D. L. Tilbrook, *Appl. Phys. Lett.* **82**, 1078 (2003).
- ⁸A. G. P. Troeman, H. Derking, B. Boerger, J. Pleikies, D. Veldhuis, and H. Hilgenkamp, *Nano Lett.* **7**, 2152 (2007).
- ⁹L. Hao, J. C. Macfarlane, J. C. Gallop, D. Cox, J. Beyer, D. Drung, and T. Schuring, *Appl. Phys. Lett.* **92**, 192507 (2008).
- ¹⁰C. Granata, E. Esposito, A. Vettoliere, L. Petti, and M. Russo, *Nanotechnology* **19**, 275501 (2008).
- ¹¹D. Vasyukov, Y. Anahory, L. Embon, D. Halbertal, J. Cuppens, L. Neeman, A. Finkler, Y. Segev, Y. Myasoedov, M. L. Rappaport, M. E. Huber, and E. Zeldov, *Nat. Nanotechnol.* **8**, 639 (2013).
- ¹²J. Nagel, O. F. Kieler, T. Weimann, R. Wolbing, J. Kohlmann, A. B. Zorin, R. Kleiner, D. Koelle, and M. Kemmler, *Appl. Phys. Lett.* **99**, 032506 (2011).
- ¹³R. Wölbling, J. Nagel, T. Schwarz, O. Kieler, T. J. Weimann, J. Kohlmann, A. B. Zorin, M. Kemmler, R. Kleiner, and D. Koelle, *Appl. Phys. Lett.* **102**, 192601 (2013).
- ¹⁴C. Granata, A. Vettoliere, R. Russo, M. Fretto, N. De Leo, and V. Lacquaniti, *Appl. Phys. Lett.* **103**, 102602 (2013).
- ¹⁵C. Granata, A. Vettoliere, M. Fretto, N. De Leo, and V. Lacquaniti, *J. Magn. Magn. Mater.* **384**, 117 (2015).
- ¹⁶M. Schmelz, Y. Matsui, R. Stolz, V. Zakosarenko, T. Schönau, S. Anders, S. Linzen, H. Itozaki, and H.-G. Meyer, *Supercond. Sci. Technol.* **28**, 015004 (2015).
- ¹⁷M. J. Martínez-Pérez, D. Gella, B. Müller, V. Morosh, R. Wolbing, J. Sesé, O. Kieler, R. Kleiner, and D. Koelle, *ACS Nano* **10**, 8308 (2016).
- ¹⁸M. Fretto, E. Enrico, N. De Leo, L. Boarino, R. Rocci, and V. Lacquaniti, *IEEE Trans. Appl. Supercond.* **23**, 1101104 (2013).
- ¹⁹C. Granata, D. Massarotti, A. Vettoliere, M. Fretto, L. D'Ortenzi, N. De Leo, D. Stornaiuolo, P. Silvestrini, B. Ruggiero, F. Tafuri, and V. Lacquaniti, *IEEE Trans. Appl. Supercond.* **26**, 1 (2016).
- ²⁰C. D. Tesche and J. Clarke, *J. Low Temp. Phys.* **29**, 301 (1977).
- ²¹Supracon AG, See <http://www.supracon.com/> for the development of low noise SQUID readout electronics.
- ²²V. Foglietti, *Appl. Phys. Lett.* **59**, 476 (1991).
- ²³J. Clarke, "SQUID concepts and systems," in *Superconducting Electronics*, edited by H. Weinstock and M. Nisenoff (Springer Verlag, Berlin/Heidelberg/New York, 1989), Vol. 59, pp. 87–148.
- ²⁴D. D. Awschalom, J. R. Rozen, M. B. Ketchen, W. J. Gallagher, A. W. Kleinsasser, R. L. Sandstrom, and B. Bumble, *Appl. Phys. Lett.* **53**, 2108 (1988).
- ²⁵M. Schmelz, V. Zakosarenko, T. Schönau, S. Anders, S. Linzen, R. Stolz, and H. G. Meyer, *Supercond. Sci. Technol.* **30**, 014001 (2017).
- ²⁶D. J. Van Harlingen, R. H. Koch, and J. Clarke, *Appl. Phys. Lett.* **41**, 197 (1982).
- ²⁷C. Granata, A. Vettoliere, P. Walke, C. Nappi, and M. Russo, *J. Appl. Phys.* **106**, 023925 (2009).
- ²⁸D. L. Tilbrook, *Supercond. Sci. Technol.* **22**, 064003 (2009).
- ²⁹R. Russo, C. Granata, E. Esposito, D. Peddis, C. Cannas, and A. Vettoliere, *Appl. Phys. Lett.* **101**, 122601 (2012).